

# High- $T_c$ and Low- $T_c$ Superconductivity in Electron Systems With Repulsion

Maxim Yu. Kagan<sup>1,2</sup> · Vitaly A. Mitskan<sup>3,4</sup> · Maxim M. Korovushkin<sup>3,5</sup>

Received: date / Accepted: date

**Abstract** We demonstrate the instability of the normal state of purely repulsive fermionic systems towards the transition to the Kohn-Luttinger superconducting state. We construct the superconducting phase diagrams of these systems in the framework of the Hubbard and Shubin-Vonsovsky models on the square and hexagonal lattices. We show that an account for the long-range Coulomb interactions, as well as the Kohn-Luttinger renormalizations lead to an increase in the critical superconducting temperatures in various materials, such as high-temperature superconductors, idealized monolayer and bilayer of doped graphene. Additionally, we discuss the role of the structural disorder and the non-magnetic impurities in superconducting properties of real graphene systems.

**Keywords** Unconventional superconductivity · Kohn-Luttinger mechanism · Graphene

**PACS** 74.20.-z · 74.20.Mn · 74.20.Rp · 74.25.Dw · 81.05.ue

## 1 Introduction

In recent years, a significant progress in experimental and theoretical investigation of high-temperature and

<sup>1</sup>P.L. Kapitza Institute for Physical Problems, 119334 Moscow, Russia

<sup>2</sup>National Research University Higher School of Economics, 109028 Moscow, Russia

<sup>3</sup>L.V. Kirensky Institute of Physics, 660036 Krasnoyarsk, Russia

<sup>4</sup>Siberian State Aerospace University, 660014 Krasnoyarsk, Russia

<sup>5</sup>Nordita, KTH Royal Institute of Technology and Stockholm University, Roslagstullsbacken 23, SE-106 91 Stockholm, Sweden

low-temperature superconducting systems with nonphonon nature of the Cooper pairing and nontrivial structure of the order parameter has been achieved. Along with the numerous studies of superconducting properties of these systems using pairing mechanisms caused by electron correlations and other exotic superconductivity mechanisms, some authors widely discuss the possibility of the development of Cooper instability in new superconducting systems using the Kohn-Luttinger mechanism, suggesting the transformation of initial repulsive interaction of two particles in vacuum into the effective attraction in the presence of the fermionic background [1–5]. In this paper, we consider the fermionic systems, such as high-temperature superconductors and monolayer and bilayer of doped graphene, in which the anomalous  $p$ -,  $d$ -, and  $f$ -wave pairing are realized, and show that in many cases the proposed mechanism results in quite high superconducting transition temperatures.

## 2 The Kohn-Luttinger Superconductivity in the Hubbard and Shubin-Vonsovsky Models

The Hubbard model [6] with the Hamiltonian

$$\hat{H} = \sum_{\mathbf{p}\sigma} (\varepsilon_{\mathbf{p}} - \mu) c_{\mathbf{p}\sigma}^\dagger c_{\mathbf{p}\sigma} + U \sum_{\mathbf{p}\mathbf{p}'\mathbf{q}} c_{\mathbf{p}\uparrow}^\dagger c_{\mathbf{p}'+\mathbf{q}\downarrow}^\dagger c_{\mathbf{p}+\mathbf{q}\downarrow} c_{\mathbf{p}'\uparrow} (1)$$

is the minimal model taking into account the band motion of electrons in a solid and strong electron interaction. Since the end of 1980s, a lot of experimental data on cuprates indicated that the main dynamics of Fermi excitations evolves in the  $\text{CuO}_2$  planes and that is why the 2D Hubbard model on a simple square lattice was mainly used to describe the nonphonon mechanisms of high- $T_c$  superconductivity. Figure 1 depicts the superconducting phase diagram of the Hubbard model. In the

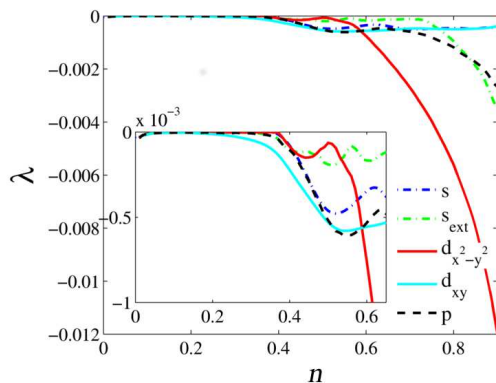


**Fig. 1** Pairing strengths for the 2D Hubbard model at  $t_2 = 0$  as a function of electron concentration.

region of low electron densities  $0 < n < 0.52$ , superconductivity with the  $d_{xy}$ -wave symmetry of the order parameter is realized [4, 7]. In the interval  $0.52 < n < 0.58$ , the strong competition between  $p$ -wave and  $d_{xy}$ -wave pairings takes place [8–10]. For  $n > 0.58$ , superconductivity of the  $d_{x^2-y^2}$ -wave type dominates [11]. It should be noted that the maximal  $T_c$  in the 2D Hubbard model was obtained in [11] in the regime  $U/W \sim 1$  ( $W$  is the bandwidth) for optimal electron concentrations  $n \sim 0.8 - 0.9$ . According to the estimation [11], the superconducting transition temperature can reach desirable values  $T_c^{d_{x^2-y^2}} \approx 100$  K, which are quite reasonable for optimally doped cuprates.

The important question concerning the role of the long-range part of Coulomb interaction in nonphonon superconductivity was considered in the paper [12]. The authors noted that previous investigations of the Kohn-Luttinger superconductivity were limited to the inclusion of the only short-range Coulomb interaction  $U$  having in mind the computational difficulties connected with taking into account the Fourier transform of the long-range Coulomb repulsion  $V_{\mathbf{q}}$  in the first- and second-order diagrams for the effective interaction [1]. The authors [12] choose the long-range Coulomb interaction  $V_{\mathbf{q}}$  in the form of the Fourier transform of the Yukawa potential which has the standard form in the 3D case:

$$V_{\mathbf{q}} = \frac{4\pi e^2}{q^2 + \kappa^2}, \quad (2)$$

where  $\kappa$  is the inverse screening length. It was concluded in [12] that small and intermediate values of  $U$  in the presence of the long-range part of Coulomb interaction do not induce realization of the Cooper instability in 3D and 2D Fermi systems in the  $p$ -wave and  $d$ -wave channels, irrespective of the value of the screening length.

To clarify the role of the long-range Coulomb interaction in the implementation of unconventional superconductivity, the authors [13] analyzed the conditions for the occurrence of the Kohn-Luttinger pairing in the 3D and 2D Shubin-Vonsovsky model (extended Hubbard model) [14] with Coulomb repulsion of electrons at the neighboring sites on the square lattice. In the momentum representation, the Hamiltonian of the model has the form

$$\hat{H} = \sum_{\mathbf{p}\sigma} (\varepsilon_{\mathbf{p}} - \mu) c_{\mathbf{p}\sigma}^\dagger c_{\mathbf{p}\sigma} + U \sum_{\mathbf{p}\mathbf{p}'\mathbf{q}} c_{\mathbf{p}\uparrow}^\dagger c_{\mathbf{p}'+\mathbf{q}\downarrow}^\dagger c_{\mathbf{p}+\mathbf{q}\downarrow} c_{\mathbf{p}'\uparrow} + \frac{1}{2} \sum_{\mathbf{p}\mathbf{p}'\mathbf{q}\sigma\sigma'} V_{\mathbf{p}-\mathbf{p}'} c_{\mathbf{p}\sigma}^\dagger c_{\mathbf{p}'+\mathbf{q}\sigma'}^\dagger c_{\mathbf{p}+\mathbf{q}\sigma'} c_{\mathbf{p}'\sigma}, \quad (3)$$

where the Fourier transform of the Coulomb interaction of electrons at the nearest sites ( $V_1$ ) and at the next-nearest sites ( $V_2$ ) in the 2D case on the square lattice yields

$$V_{\mathbf{q}} = 2V_1(\cos q_x + \cos q_y) + 4V_2 \cos q_x \cos q_y. \quad (4)$$

The last term in the Hamiltonian (3) reflects the fact that the screening radius in the systems may be by several times larger than the unit cell parameter. It demonstrates an advantage of the Shubin-Vonsovsky model, in which the intersite Coulomb interaction is taken into account within several coordination spheres.

In [13], instead of Yukawa potential used as the Fourier transform of the intersite interaction, the case of extremely strong Coulomb repulsion was considered. In this case, the Shubin-Vonsovsky model becomes the most repulsive and the most unbeneficial model for superconductivity. However, the previous results [3, 4] for the Kohn-Luttinger superconducting  $p$ -wave pairing being attained both in the 2D and 3D Hubbard model and the same expressions for  $T_c$ , as in the case of  $V_1 = 0$ , were obtained [13]. An account for  $V_1$  changes only the preexponential factor. Therefore, superconducting  $p$ -wave pairing can be always realized in the Fermi systems with pure Coulomb repulsion in the absence of electron-phonon interaction.

A similar analysis was carried out by the authors [9] for the extended Hubbard model in the Born weak-coupling approximation ( $W > U > V_1$ ). In the calculation [9] of the effective interaction of electrons, the intersite Coulomb interaction was taken into account only in the first order of perturbation theory in the form (4) and the polarization contributions included only the terms of the order  $U^2$ . It was shown that the long-range interaction has a tendency to suppress unconventional pairing in some channels; nevertheless the Kohn-Luttinger superconductivity survives in whole range of electron densities  $0 < n < 1$  and for all the relations between the model parameters.

The results of [9] suggest to study the conditions for the appearance of the Kohn-Luttinger instability taking into account all the second-order terms in the long-range Coulomb interaction. In [10], we considered the effect of the Coulomb interaction of electrons  $V_1$  and  $V_2$  on the realization of the Cooper instability in the framework of the Shubin-Vonsovsky model in the Born weak-coupling approximation. Since the polarization effects are manifested through the second-order contributions in  $V$ , to account for the Kohn-Luttinger effects connected with the intersite Coulomb repulsion, we used the complete expression for the effective interaction

$$U_{eff}(\mathbf{p}, \mathbf{q}) = U_{eff}^{(I)}(\mathbf{p}, \mathbf{q}) + U_{eff}^{(U^2)}(\mathbf{p}, \mathbf{q}) + U_{eff}^{(UV)}(\mathbf{p}, \mathbf{q}) + U_{eff}^{(V^2)}(\mathbf{p}, \mathbf{q}). \quad (5)$$

In this case, the polarization effects proportional to  $UV$  and  $V^2$  considerably modify and complicate the structure of the superconducting phase diagram (Fig. 2a). With the increase of the parameter  $V_1$  of the intersite Coulomb interaction, only the three phases corresponding to the  $d_{xy}$ -wave,  $p$ -wave, and  $s$ -wave types of symmetry of the superconducting order parameter are stabilized. Note that in the range of high electron densities and for  $0.25 < V_1/|t_1| < 0.5$ , the Kohn-Luttinger polarization effects lead to the occurrence of the unconventional  $s$ -wave pairing [5, 10, 18].

Despite their parametric smallness, the second-order effects in  $V$  represent the decisive contribution to superconductivity in the Shubin-Vonsovsky model. To answer the question why the first-order contributions in  $V$  do not suppress the second-order contributions, it is necessary to compare the different partial contributions to the total effective interaction. The histogram in Fig. 2b reflects the results for a point of the phase diagram in which the superconducting phase with the  $s$ -wave symmetry of the order parameter corresponds to the ground state. Matrix elements of the effective interaction  $\{U_{eff}\}_{mn}$  calculated for small  $m$  and  $n$  are presented here in the histogram. The values of the matrix elements for  $n, m > 2$  are not given because of their smallness. One can see from the histogram that, for the chosen parameters, the first- and the second-order contributions  $U_{eff}^{(I)}$  and  $U_{eff}^{(U^2)}$ , respectively, give only positive values of the matrix elements, and thus correspond to repulsion. It means that an account of only these processes would not lead to the  $s$ -wave superconducting pairing. Similarly, the second-order contributions  $U_{eff}^{(UV)}$  also would not give rise to superconductivity, and only the second-order contributions  $U_{eff}^{(V^2)}$  provide the negative values of the matrix elements  $\{U_{eff}\}_{mn}$  (and as a result, the negative eigenvalues of  $\lambda$ ) leading

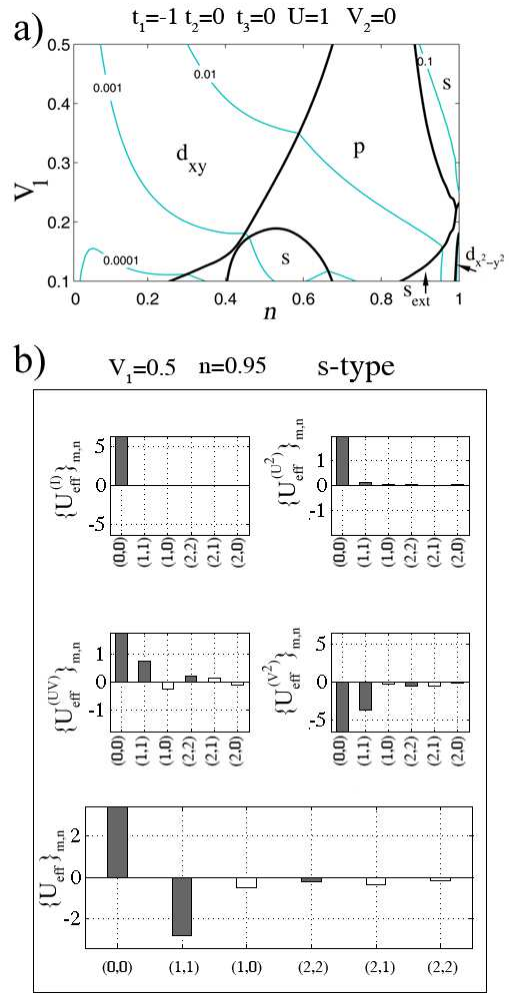


**Fig. 2** Phase diagram of the Shubin-Vonsovsky model, constructed taking into account the second-order contributions in  $V$  for the set of parameters  $t_2 = t_3 = 0$ ,  $U = 1$  (blue curves show the lines of constant values of  $|\lambda|$ ) (a) and the values of the matrix element for partial contributions  $U_{eff}^{(I)}$ ,  $U_{eff}^{(U^2)}$ ,  $U_{eff}^{(UV)}$ ,  $U_{eff}^{(V^2)}$  as well as the resulting effective interaction  $\{U_{eff}\}_{mn}$  for  $V_1 = 0.5$  and  $n = 0.95$  (b).

to the realization of the superconducting  $s$ -wave pairing.

Thus, the long-range Coulomb repulsion in the lattice models usually contribute only to the certain pairing channels and does not affect the other channels. At the same time, the polarization contributions described by the Kohn-Luttinger diagrams possess the components in all the channels, and more than one of them usually plays in favor of attraction. In such a situation, the long-range Coulomb repulsion probably either does not affect at all the main component of the effective interaction, which leads to pairing, or it suppresses the principal component without affecting the secondary ones [9, 10].

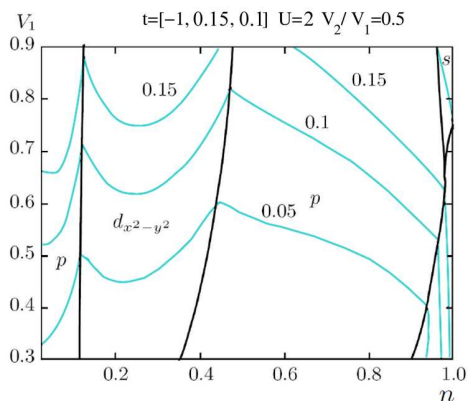


**Fig. 3** Phase diagram of the Shubin-Vonsovsky model calculated for the parameters  $t_2 = 0.15$ ,  $t_3 = 0.1$ ,  $U = 2$ , and  $V_2/V_1 = 0.5$  (all the parameters are in units of  $|t_1|$ ). Blue curves are the lines of constant value of  $|\lambda|$ .

The same scenario of superconductivity is also observed in the  $p$ -wave channel in the phase diagram (Fig. 2a).

In [10], the effect of the distant electron hoppings  $t_2$  and  $t_3$  on the superconducting phase diagram was analyzed. It is known that an account for these hoppings can considerably modify the density of states (DOS) and shift the Van Hove singularity (VHS) away from the half-filling to the region of the lower (or higher) electron densities. Figure 3 shows the modification of the phase diagram of the Shubin-Vonsovsky model, which is observed upon an increase in  $U$ . It can be seen that in the range of low electron densities, as well as in the range of densities close to the VHS, the  $d_{x^2-y^2}$ -wave pairing is achieved with quite large values of  $|\lambda| \sim 0.1 - 0.2$ . This result is important for analyzing the possibility of the realization of the Kohn-Luttinger mechanism in high- $T_c$  superconductors. It should be noted that for  $|\lambda| \sim 0.2$ , the superconducting transition temperatures can reach the values  $T_c^{d_{x^2-y^2}} \sim 100$  K which are quite reasonable for cuprates.

### 3 The Kohn-Luttinger Superconductivity in Idealized Monolayer and Bilayer Graphene

At the present time, the possible development of superconductivity in the framework of the Kohn-Luttinger mechanism in graphene under appropriate experimental conditions is widely discussed. Despite the fact that intrinsic superconductivity so far has not been observed in graphene, the stability of the Kohn-Luttinger superconducting phase has been investigated and the symmetry of the order parameter on the hexagonal lattice was identified. It was found [15] that chiral supercon-

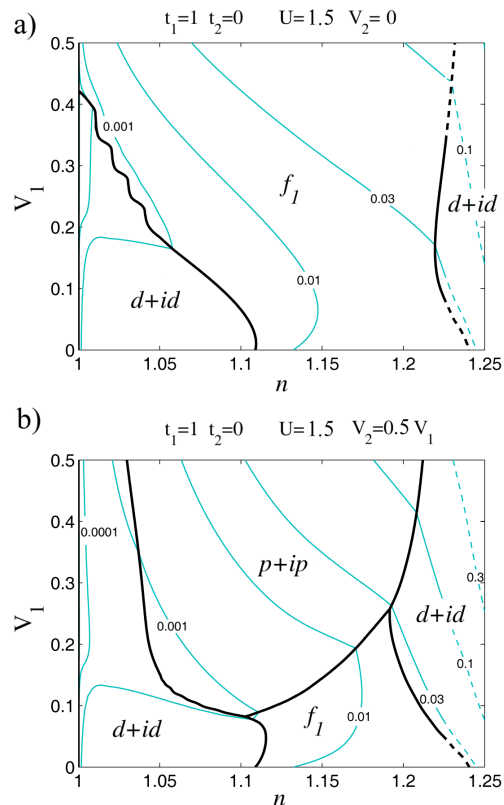


**Fig. 4** (Color online) Phase diagram of the superconducting state of the graphene monolayer at  $U = 1.5|t_1|$  for (a)  $V_2 = 0$  and (b)  $V_2 = 0.5V_1$ . Blue curves show the lines of the constant values of  $|\lambda|$ .

ductivity [16] with the  $d + id$ -wave symmetry of the order parameter prevails in a large domain near the VHS in the DOS [17]. The competition between the superconducting phases with different symmetry types in the wide electron density range  $1 < n \leq n_{VH}$ , where  $n_{VH}$  is the Van Hove filling, in graphene monolayer was studied in papers [18,19]. It was demonstrated that at intermediate electron densities the Coulomb interaction of electrons located on the nearest carbon atoms facilitates implementation of superconductivity with the  $f$ -wave symmetry of the order parameter, while at approaching the VHS, the superconducting  $d + id$ -wave pairing evolves [18,19].

Using the Shubin-Vonsovsky model in the Born weak-coupling approximation, we investigated the role of the Coulomb repulsion of electrons located at next- nearest neighboring carbon atoms for the development of the Kohn-Luttinger superconductivity in an idealized graphene monolayer disregarding the effect of the Van der Waals potential of the substrate and both magnetic and non-magnetic impurities. Figure 4a shows the calculated phase diagram of the Kohn-Luttinger superconducting state in graphene monolayer as a function of the

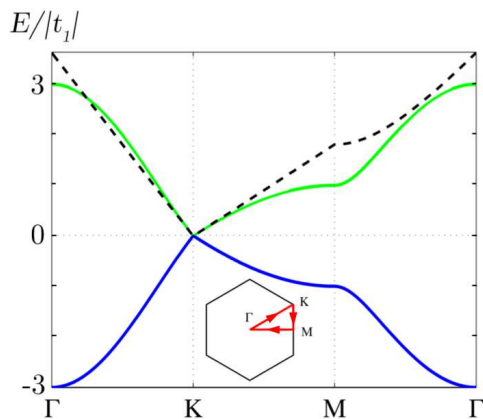


**Fig. 5** (Color online) Energy spectra of graphene monolayer (blue and green solid lines) and energy spectra obtained in the framework of the Dirac approximation (black dashed line). Subplot depicts the path around the Brillouin zone.

carrier concentration  $n$  and  $V_1$  for the set of parameters  $U = 1.5|t_1|$ , and  $V_2 = 0$ . It can be seen that the phase diagram consists of three regions. At low electron densities  $n$ , the ground state of the system corresponds to the chiral superconductivity with the  $d + id$ -wave symmetry of the order parameter [17]. At the intermediate electron densities, the superconducting  $f$ -wave pairing is implemented. At the large values of  $n$ , the domain of the superconducting  $d + id$ -wave pairing occurs [15]. With the increase of the parameter  $V_1$  of the intersite Coulomb interaction, in the region of small values of  $n$ , the  $d + id$ -wave pairing is suppressed and the pairing with the  $f$ -wave symmetry of the order parameter is implemented. Thin blue lines in Fig. 4 are the lines of the equal values of the effective coupling constant  $|\lambda|$ . It can be seen that in this case in the vicinity of  $n_{VH}$  the effective coupling constant reaches the values of  $|\lambda| = 0.1$ .

Let us consider the modification of the phase diagram for graphene monolayer with respect to the Coulomb interaction  $V_2$  between the electrons located at the next-nearest carbon atoms. It can be seen in Fig. 4b for the fixed ratio between the parameters of the long-range Coulomb interactions  $V_2 = 0.5V_1$  that when  $V_2$  is taken into account, the phase diagram changes qualitatively. These changes involve the suppression of a large region of the  $f$ -wave pairing at the intermediate electron densities and the implementation of the chiral superconducting  $p + ip$ -wave pairing. In addition, when  $V_2$  is taken into account, the effective coupling constant increases to the values of  $|\lambda| = 0.3$ . Consequently, it leads to a significant increase in  $T_c$  in idealized doped graphene. Note that here we do not analyze the account for the electron hoppings to the next-nearest carbon atoms  $t_2$ ,

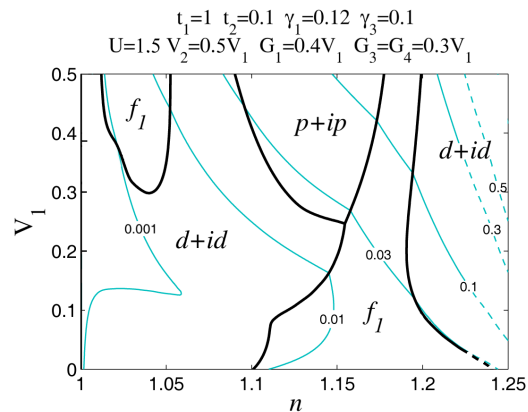


**Fig. 6** Phase diagram of the superconducting state of graphene bilayer shown as a function of the variables " $n - V_1$ " at  $t_2 = 0.1$ ,  $\gamma_1 = 0.12$ ,  $\gamma_3 = 0.1$ ,  $U = 1.5$ ,  $V_2 = 0.5V_1$ ,  $G_1 = 0.4V_1$ ,  $G_3 = G_4 = 0.3V_1$  (all the parameters are in units of  $|t_1|$ ).  $G_1$ ,  $G_3$  and  $G_4$  are the parameters of the interlayer Coulomb repulsion,  $\gamma_1$  and  $\gamma_3$  are the interlayer hoppings. Blue curves are the lines of the constant values of  $|\lambda|$ .

since an account for these hoppings for graphene monolayer does not significantly modify the DOS in the carrier concentration regions between the Dirac point and both VHS points  $n_{VH}$  [18].

It should be noted also that the Kohn-Luttinger superconductivity in graphene never develops near the Dirac points. The calculations show that in the vicinity of these points, where the linear approximation for the energy spectrum of graphene monolayer works pretty well, the DOS is very low and the effective coupling constant  $|\lambda| < 10^{-2}$ . The higher values of  $|\lambda|$ , which are indicative of the development of the Cooper instability at reasonable temperatures, arise at the electron densities  $n > 1.15$ . However, at such densities, the energy spectrum of the monolayer along the direction  $KM$  of the Brillouin zone (Fig. 5) already significantly differs from the Dirac approximation.

Since the electronic properties of graphene depend on the number of carbon layers [20], we analyzed the possibility of implementation of the Kohn-Luttinger superconductivity and constructed the phase diagram (Fig. 6) in idealized graphene bilayer [21]. The calculation shows that the separate increase of the parameters of the interlayer Coulomb repulsion  $G_3$  and  $G_4$  suppresses the  $d + id$ -wave pairing and, at the same time, broadens the  $f$ -wave pairing region at small electron densities. The superconducting  $d + id$ -wave phase is suppressed the most effectively by enhancing the parameter  $G_4$  of the interlayer Coulomb interaction. When the interactions  $G_3$  and  $G_4$  are simultaneously taken into account, then along with the intensive suppression of the superconducting  $d + id$ -wave pairing at small electron den-

sities and the implementation of the superconductivity with the  $f$ -wave symmetry of the order parameter, the growth of the absolute values of effective coupling constant  $\lambda$  is also observed.

#### 4 The Kohn-Luttinger superconductivity in real graphene

Our calculation showed that the Kohn-Luttinger mechanism can lead to the superconducting transition temperatures  $T_c \sim 10 \div 20$  K in an idealized graphene monolayer and  $T_c \sim 20 \div 40$  K in an idealized graphene bilayer. Contrary to these rather optimistic estimations, in real graphene, superconductivity has not been found yet. This material is only close to superconductivity.

The reason for that is probably connected with the effects of structural disorder and the presence of the nonmagnetic impurities in real graphene (or graphite). Note that for exotic ( $p$ -,  $d$ - and  $f$ -wave) as well as for  $s$ -wave superconducting pairing with nodal points on the 2D lattice ( $\Delta_s(\phi) \sim \cos 6n\phi$ ,  $\Delta_{s_{ext}}(\phi) \sim \sin 6n\phi$ ,  $n \geq 1$ ) the Anderson theorem [22] for nonmagnetic impurities is violated and anomalous superconductivity can be suppressed for  $\gamma \geq k_B T_c^{clean}$  [23–25], where  $\gamma = \hbar/(2\tau)$  is an electron damping due to scattering on impurities. In another words,  $k_B T_c^{clean} \leq \hbar p_F / ml$ , where the Fermi-momentum  $p_F$  is connected with a 2D electron density  $n_{2D}$  in graphene ( $p_F \sim \hbar \sqrt{2\pi n_{2D}}$ , if we assume the circular Fermi-surface for simplicity). At the same time,  $l$  is an effective mean-free path extracted both from transport and Hall measurements and thus taking into account both the effects of the structural disorder and the presence of the nonmagnetic impurities.

To our best knowledge, the record experimental parameters available nowadays correspond to  $\max(l) \sim 2 \cdot 10^3 \text{ \AA}$  and  $\max(n_{2D}) \sim 10^{13} \text{ cm}^{-2}$  in real graphene monolayers. The maximal values of the mean-free path today still correspond to the moderately clean case. The corresponding amount of disorder for the high density  $n_{2D} \sim 10^{13} \text{ cm}^{-2}$  is sufficient to suppress totally anomalous  $T_c$  of the order of 10 K. This experimental challenge for the discovery of superconductivity in real graphene is to further increase the 2D electron density or to prepare the ultraclean graphene monolayer or bilayer. Another possibility for getting closer to realization of superconductivity in real graphene is to perform the experiments on quasi 1D epitaxial graphene nanoribbons [26]. In this case, however, the competition between superconductivity and the Peierls-type of instabilities is highly possible, at least on the level of theoretical considerations in the framework of parquet diagrammatic approximation [27].

**Acknowledgements** The authors are grateful to V. V. Val'kov, M. V. Feigel'man and A. Ya. Tzalenchuk for valuable remarks. This work is supported by the Russian Foundation for Basic Research (nos. 14-02-00058 and 14-02-31237). One of the authors (M. Yu. K.) gratefully acknowledges support from the Basic Research Program of the National Research University Higher School of Economics. Another one (M. M. K.) thanks the scholarship SP-1361.2015.1 of the President of Russia and the Dynasty foundation.

#### References

1. Kohn, W., Luttinger, J. M.: Phys. Rev. Lett. **15**, 524 (1965)
2. Fay, D., Layzer, A.: Phys. Rev. Lett. **20**, 187 (1968)
3. Kagan, M. Yu., Chubukov, A. V.: JETP Lett. **47**, 614 (1988)
4. Baranov, M. A., Chubukov, A. V., Kagan, M. Yu.: Int. J. Mod. Phys. B **6**, 2471 (1992)
5. Kagan, M. Yu., Mitskan, V. A., Korovushkin, M. M.: Phys. Usp. **58** (8) (2015)
6. Hubbard, J. C.: Proc. R. Soc. London A **276**, 238 (1963)
7. Baranov, M. A., Kagan, M. Yu.: Z. Phys. B: Condens. Matter **86**, 237 (1992)
8. Hlubina, R.: Phys. Rev. B **59**, 9600 (1999)
9. Raghu, S., Berg, E., Chubukov, A. V., Kivelson, S. A.: Phys. Rev. B **85**, 024516 (2012)
10. Kagan, M. Yu., Val'kov, V. V., Mitskan, V. A., Korovushkin, M. M.: JETP Lett. **97**, 226 (2013); JETP **117**, 728 (2013)
11. Raghu, S., Kivelson, S. A., Scalapino, D. J.: Phys. Rev. B **81**, 224505 (2010)
12. Alexandrov, A. S., Kabanov, V. V.: Phys. Rev. Lett. **106**, 136403 (2011)
13. Kagan, M. Yu., Efremov, D. V., Marienko, M. S., Val'kov, V. V.: JETP Lett. **93**, 720 (2011)
14. Shubin, S., Vonsowsky, S.: Proc. Roy. Soc. A **145**, 159 (1934)
15. Nandkishore, R., Levitov, L. S., Chubukov, A. V.: Nature Phys. **8**, 158 (2012)
16. Volovik, G. E.: *Exotic properties of superfluid  $^3\text{He}$* , World Scientific, Singapore, 1992.
17. Black-Schaffer, A. M., Honerkamp, C.: J. Phys.: Condens. Matter **26**, 423201 (2014)
18. Kagan, M. Yu., Val'kov, V. V., Mitskan, V. A., Korovushkin, M. M.: Solid State Commun. **188**, 61 (2014)
19. Nandkishore, R., Thomale, R., Chubukov, A. V.: Phys. Rev. B **89**, 144501 (2014)
20. Guinea, F., Castro Neto, A. H., Peres, N. M. R.: Phys. Rev. B **73** 245426 (2006)
21. Kagan, M. Yu., Mitskan, V. A., Korovushkin, M. M.: Eur. Phys. J. B **88**, 157 (2015)
22. Anderson, P. W.: J. Phys. Chem. Solids **11**, 26 (1959)
23. Abrikosov, A. A., Gor'kov, L. P.: Sov. Phys. JETP **12**, 337 (1961)
24. Abrikosov, A. A., Gor'kov, L. P., Dzyaloshinski, I. E.: *Quantum Field Theory in Statistical Physics*, Prentice Hall, Englewood Cliffs, New Jersey, 1963
25. Posazhennikova, A. I., Sadovskii, M. V.: JETP Lett. **63**, 358 (1996)
26. Baringhaus, J., Ruan, M., Edler, F., et al.: Nature **506**, 349 (2014)
27. Bychkov, Yu. A., Gor'kov, L. P., Dzyaloshinskii, I. E.: Sov. Phys. JETP **23**, 489 (1966)